IRANIAN JOURNAL OF CATALYSIS

Preparation and Characterization of WO_3 Nanosheets and Au/WO_3 Nanocomposite for Rabid Photocatalytic degradation of methylene blue dye

Fatima Allawi Abdul Sajad[a*], Hanaa Kadtem Egzar [a*], Mazin Auny Mahdi [b]

a) Department of Chemistry, College of Science, University of Kufa, Najaf, Iraq

b) Department of Physics, College of Science, University of Basrah, Basra, Iraq

Received 29 May 2023; received in revised form 8 September 2023; accepted 23 September 2023 (**DOI: 10.30495/IJC.2023.1987426.2010**)

ABSTRACT

The sol-gel technique is employed for the synthesis of tungsten trioxide (WO_3) nanosheets. The Au/WO_3 nanocomposite is prepared using laser ablation employing an Nd-YAG laser operating at a wavelength of 1064 nm and utilizing gold metal. The SEM images demonstrate that WO_3 was formed as nanosheets with a thickness between 36nm and 80nm. X-ray diffraction (XRD) patterns confirmed the monoclinic crystal structure and high crystallinity of the WO_3 structure. The optical absorption of both WO_3 nanosheets and Au/WO_3 nanocomposite exhibited a pronounced absorption edge, with an energy gap of 2.52 eV and 2.41 eV, respectively. The photocatalytic activity of WO_3 nanosheets and Au/WO_3 nanocomposite was determined by degrading Methylene blue (MB) dye under visible light irradiation using different catalyst doses and pH values. The WO3 nanosheets and Au/WO_3 nanocomposites that were prepared demonstrate a fast degradation of MB dye. The highest photodegradation efficiency (PDE) of MB dye was 75.9% when 0.05 g of Au/WO_3 nanocomposite was exposed to 7 pH for 6 min of irradiation. Nevertheless, an increase of pH led to a corresponding rise in PDE. Particularly, the PDE values reached 85.5% and 95.7% when using 0.1 g of WO_3 nanosheets and Au/WO_3 nanocomposite, respectively, under the conditions in a pH level of 12 and an irradiation duration of 6 minutes.

***Keywords**: Au/WO_3, Nanosheets, Nanocomposite, Photodegradation, Methylene blue dye*

1. Introduction

Polluted water, particularly water contaminated with organic contaminants, causes diseases in humans, killing a few million people each year, and the death rate is expected to rise in the coming years due to growing water pollution [1]. Thus, one of the most pressing issues confronting the human living system is the removal of organic contaminants from wastewater. However, a variety of viable approaches for removing these contaminants have been documented, including advanced oxidation processes (AOPs), biological degradation, and adsorption [2]. Nano-semiconductor photocatalysts showed a suitable way for removing the numerous organic impurities from water due to a simply degraded below UV or solar light radiation in the presence of photocatalysts [3, 4]. The main problem of pure semiconductor photocatalysts is the fast recombination rate of photogenerated electron–hole pairs which leads to a decrease the photocatalytic efficiency [5, 6]. However, the most successful ways to circumvent this limitation are to support and couple two or more semiconductors, such as p-n, n-n, or p-p hetero-junction structures [7, 8]. However, A. Yousefi and A. Nezamzadeh-Ejhieh outlined many strategies that can be used to slow or prevent e/h recombination which in turn led to an increase in the photocatalyst efficiency [9]. For example, a nano-sized strategy that helps electrons and holes to travel and precipitate on the surface of the semiconductor and then degradation dyes through redox and oxidant process. The other method is doping metal oxide by metals or nonmetals elements which create another energy level inside the system for occupations by e and h which in turn led to prevent its recombination. Furthermore, the plasmonic way is another strategy for enhancing the separation of the charge carriers in the photoexcited semiconductors.

*Corresponding author:
E-mail address: *fatimaa.muhammad@uokufa.edu.iq* (**F. Allawi**); hanaak.abdullah@uokufa.edu.iq (**H. Kadtem**)

metal oxide/metal core-shells such as Ag/ZnO nanostructures can be effectively used to enhance the photodegradation percentage through absorb visible light and also slow e/h recombination [10]. Tungsten trioxide (WO_3) has a narrow bandgap of 2.4–2.8 eV and enhanced photocatalytic oxidation ability at the valence band (VB) edge potential; consequently, it has significant advantages in visible light photocatalytic degradation. WO_3 has the most stable crystal structure of all tungsten-based oxides, as well as low toxicity, a wide source, strong resistance to photo corrosion, and excellent recycling performance [11]. Like to other metal oxides, WO_3 is not consistently useful as a photocatalyst due to the fast e and h recombination rate (e-/h+). However, preparing WO_3 nanocomposite with the semiconductors such as ZnO or CdS can be slow the recombination rate of e/h that led to enhance photocatalyst efficiency [12, 13]. Furthermore, loading a metal on the surface of WO_3 led to enhance photocatalytic action of WO_3 due to they be able to afford the electron combine which ran to sufficient negative potentials of O2 reduction[10]. Platinum (Pt), gold (Au), and silver (Ag) are used to modify the surface of WO3 and improve the photodegradation percentage under visible light [14-16]. In this study, the sol-gel method is used to prepare WO_3 nanosheets that are covered by Au nanoparticles that are prepared by laser ablation to fabricate Au/WO_3 nanocomposite. The prepared samples are used for rabid degradation of methylene blue (MB) dye under visible light irradiation using different catalyst doses and pH.

2. Experimental

2.1. Materials

Tungsten hexachloride (WCl_6) is used as a source to tungsten ions (W^{+6}) while ethanol (C_2H_5OH) is used to produce the tungsten alkoxide precursor [$W(OC_2H_5)_6$], ammonium hydroxide (NH_4OH) as base catalyzed in the hydrolysis of metal alkoxides to results in formation of metal hydroxides which calcinated to produce metal oxides. Moreover, the photodegradation efficiency of the produced samples is determined using Methylene blue dye with a concentration of 20 parts per million (ppm). All materials are purchased from Merck Company. A high purity of 99.9 of gold (Au) sheet with a dimension of 0.6 × 0.9 cm^2 is used to prepare Au nanoparticles using laser ablation method

2.2. Preparation of WO_3 nanosheets

Sol-gel process is used to produce the tungsten trioxide nanomaterial as described in previous work [13]. At first, 7 g of WCl_6 (Acros Organics) was mixed with 100 ml of C_2H_5OH to prepare tungsten alkoxide [$W(OC_2H_5)_6$] precursor. Then, 10 ml of 0.5 M of NH_4OH solution was added to the precursor as a catalyst, and the solution was stirred for 24 h with cooling by ice while the hydrolysis and condensation processes occurred. The chloride ions were then removed from the product by adding 0.1M of $AgNO_3$ solution that led to produce AgCl in the product which in turn was removed by washing the precipitate by deionized water (DIW) and centrifuging until totally remove the AgCl from the precipitate. Finally, the prepared precipitate is evaporated by adding ammonia hydroxide and calcined at 500 °C for 1h.

2.3. Preparation of Au Nanoparticles and Au/WO_3 nanocomposite

In this study, a high-purity gold sheet sized (0.6 × 0.6) cm^2 was utilized as the starting material for the formation of gold nanoparticles (AuNPs) using the laser ablation method. Nd-YAG laser with a wavelength of 1064 nm, pulse width of 10 ns, energy of 800 mJ / pulse, and 3 Hz frequency was used to ablate Au NPs. A Sheet of Au was immersed in a vessel contains 2 ml of DIW and the distance between the sheet and laser was 7cm. The Au sheet was ablated by 180 pulses of laser and upon irradiation of the laser beam, the color of the solution gradually turned to pale red indicating to form of Au nanoparticles[15]. To prepare Au/WO_3 nanocomposite, the laser ablation method is used also at the same conditions which utilized to synthesis Au nanoparticles. The Au sheet is immersed in a 10ml suspension of WO_3 NPs under continuous stirring. To determine the mass of gold removed from the gold target, the target was weighed before and after ablation, by 180 pulses of laser [16] mass was measured to within 0.0001g.

2.4. Evaluation of Photocatalytic Activity

Photocatalytic activity of prepared WO_3 nanosheets and Au/WO_3 nanocomposite was studied through the degradation of methylene blue (MB) dye that was utilized as an organic contaminant. In a characteristic reaction, 0.1 g of the catalyst material was added to 20 ppm of 50 ml MB dye solution. The catalyst/ dye solution was stirred magnetically in the dark for 10 min to attain adsorption equilibrium. Subsequently, the solution had irradiation using a 500 W tungsten lamp positioned at a distance of approximately 20 cm from the solution. A volume of 3 mL of the solution was extracted at every one minute and subjected to centrifugation in order to remove the catalyst particles. The absorbance of catalyzed solution was measured by

UV-Vis spectrophotometer (Shimadzu, UV-1800 Å). The investigation of the effect of pH on dye degradation holds significance due to the discharge of dyes into effluent at diverse pH levels. The study involved conducting experiments at different pH levels, particularly spanning from 4 to 12. A dye concentration of 20ppm was maintained throughout the experiments, and the pH levels were changed by adding either 0.1M HCl or 0.1M NaOH. The objective of these experiments was to investigate the influence of pH on the efficiency of dye solution degradation. Furthermore, different catalyst quantities of 0.01-0.25 g are used to catalyze MB dye. The photodegradation efficiency (PDE) of MB dye solution after treatment by light was determined using the equation [17]:

$$P.D.E = \frac{C_o - C}{C_o} 100 \qquad (1)$$

Where C_o and C are the initial concentration and the concentration of dye at a certain irradiation time of MB dye, respectively.

2.5. Characterization Tooles

The surface morphology and crystalline structure of the WO_3 nanostructure and Au/WO_3 nanocomposite were performed using Field-Emission Scanning Electron Microscopy (FESEM) type NanoNova 450, FEI, The Netherland and X-ray diffraction analysis (XRD) (XPert PRO MPD with CuKα radiation., PANalytical, The Netherlands). The optical absorption was conducted using a Shimadzu UV–vis spectrophotometer model UV-1800 (Japan).

3. Results and Discussion

3.1. Structural properties

Structural properties of prepared WO_3 nanosheets and Au/WO_3 nanocomposite were studied through XRD technique as shown in **Fig.1**. The XRD pattern of WO_3 in Fig.1a was appeared diffraction peaks at 2θ of 22.9, 23.49, 24.2, 26.48, 28.61, 33.2, 34.5, 36.1, 42, 45.1, 48.45, 49.78, 54.9, 55.72, 61.5 corresponding to lattice planes of (002), (020), (200), (120), (112), (022), (202), (122), (222), (032), (004), (400), (024), (113), and (133) respectively, of monoclinic crystal structure of WO_3 (JCPDS no 43–1035) [17,18]. The sharpness of the major XRD peaks indicated that the prepared WO_3 had a high degree of crystallinity. By comparing the XRD pattern of the Au/WO_3 nanocomposite and WO_3, it is proved that Au has loaded in WO_3 during the synthesis reaction and the intensity of the peak decreases after the loading of Au nanoparticles in WO_3 and appears a new diffraction peak at 2θ of 38.15o corresponding to FCC crystal structure of Au NPs [19]. The average crystalline size of prepared WO_3 nanosheets was estimated by the Scherer formula [20]:

$$D = \frac{0.94\,\lambda}{\beta cos\vartheta} \quad 2$$

where D is the average crystalline size, λ is wavelength in angstrom, β is the FWHM in radian and θ is the diffraction angle in degree. The value of D was 36.0 nm that calculated depending on the highest intensity diffraction peak for the (020) plane, while D for Au NPs was 37.2nm.

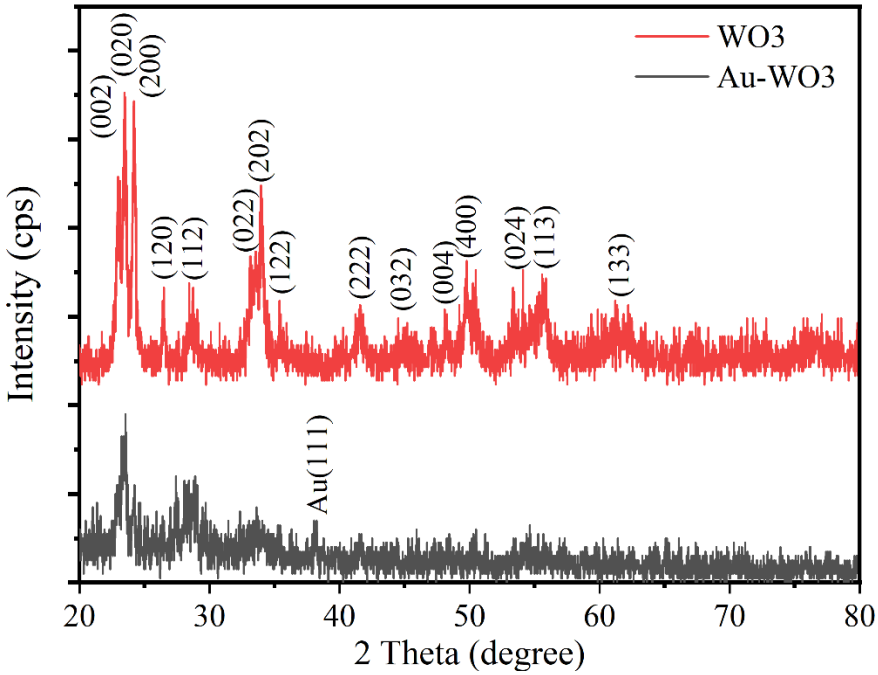

Fig. 1: XRD pattern of WO_3 and Au/WO_3 nanocomposite

3.2. Surface Morphology

Fig. 2 depicts FE-SEM images of WO_3 nanosheets and Au/WO_3 nanocomposite that have been prepared. **Fig. 2a** displays FE-SEM images confirming that WO_3 was formed as nanosheets with a thickness ranging from 36nm to 80nm. As depicted in **Fig. 2b**, the Au NPs are encased by the prepared WO_3 nanosheets. **Fig. 3** shows the TEM images of prepared WO_3 nanosheets and Au/WO_3 nanocomposite. The TEM image of Au nanoparticles confirmed spherical shape with around 30nm diameter (**Fig.3a**) while WO_3 are formed as nanosheets with appearing some of nanoparticles as shown in **Fig.3b**. The TEM image of Au/WO_3 nanocomposite showed that the Au NPs are good distributed on the surface WO_3 nanosheets. Further, nanosheets and nanoparticles with various shapes also appeared in TEM image of Au/WO_3 nanocomposite (**Fig.3c**). **Fig. 4a** and **b** depict the EDX spectra of the prepared WO_3 nanosheets and Au/WO_3 nanocomposite samples. However, W, O, and Au had quantities of 25.06%, 73.84 %, and 1.1%, respectively. With an O/W ratio of 2.94, the prepared WO_3 nanosheets are stoichiometric. **Fig. 4c** illustrates an elemental imaging image of the nanocomposite Au/WO_3. These elemental mapping images demonstrate the sample's relatively uniform distribution of W and O atoms. Additionally, AuNPs are dispersed and covered the surface of WO_3 nanosheets.

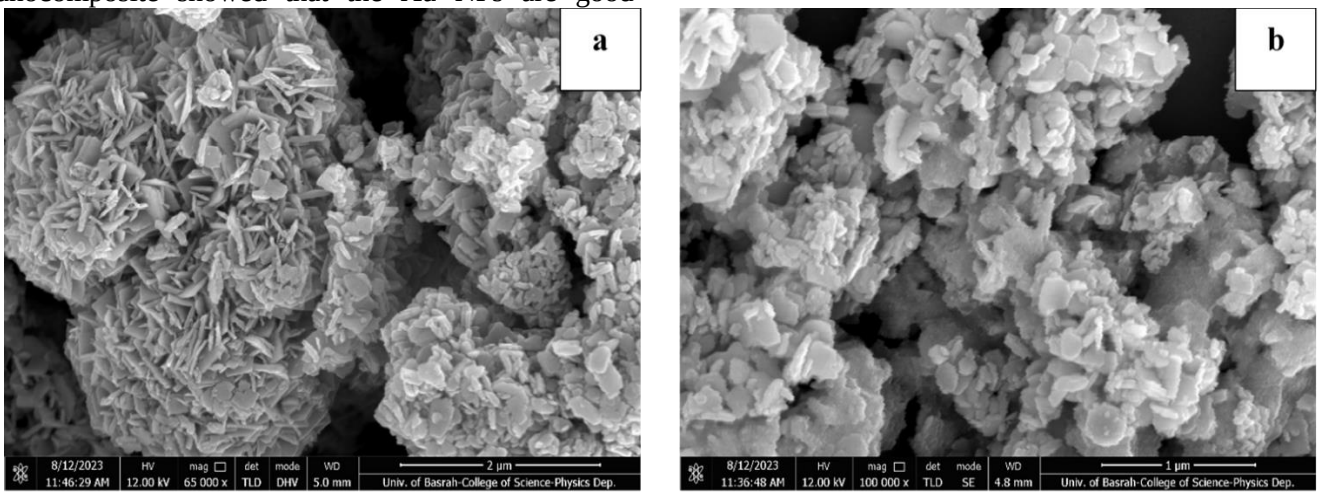

Fig. 2: FE-SEM images of prepared (a) WO_3 nanosheets and (b) Au/WO3 nanocomposite

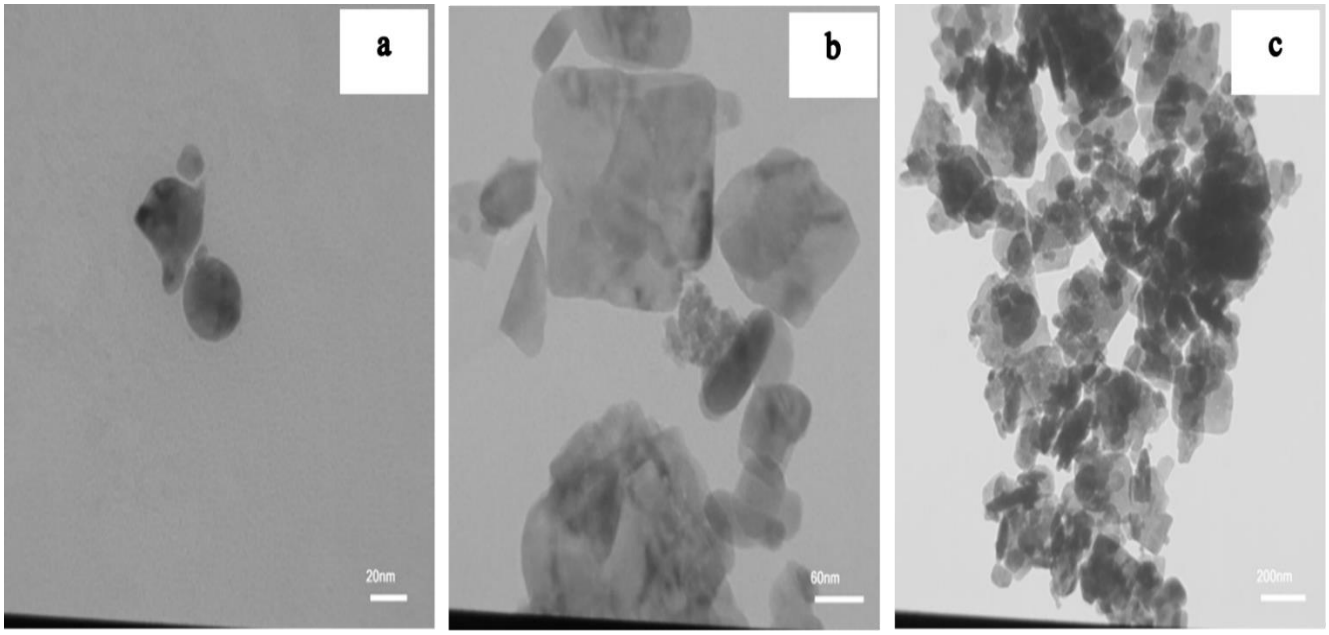

Fig. 3: TEM images of prepared (a) Au NPs, (b) WO_3 nanosheets, and (c) Au/ WO_3 nanocomposite

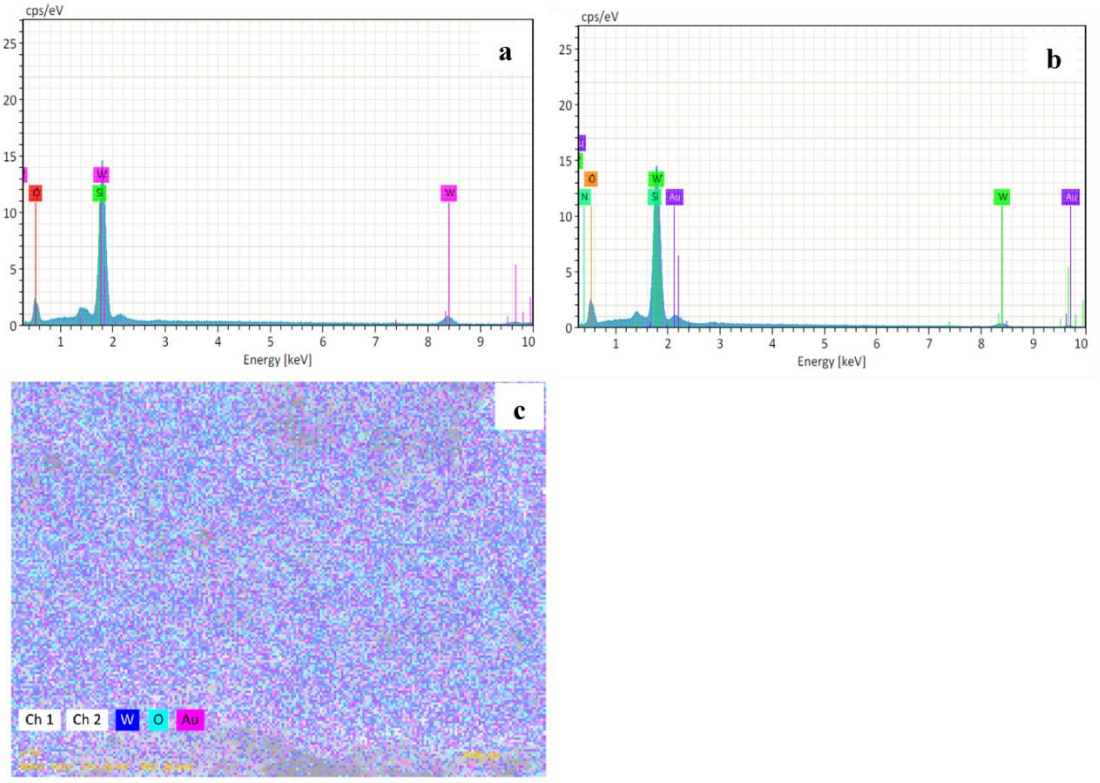

Fig. 4: EDX spectra of prepared (a) WO_3 nanosheets, (b) Au/WO_3 nanocomposite, and (c) elemental mapping images of Au/WO_3 nanocomposite

3.3. Optical properties

The absorption spectra of WO_3 nanosheets and Au/WO_3 nanocomposite have been recorded in the wavelength range of 300-900 nm as shown in **Fig. 5**. The absorption spectra of prepared samples confirmed that the Au/WO_3 nanocomposite appeared to higher absorption value in the whole spectrum range from UV to visible region compared by WO_3 nanosheets. The optical band gap was obtained following the Kubelka-Munk equation [21]:

$$\alpha h\upsilon = \beta(h\upsilon - Eg)^n \quad (3)$$

Where β is a constant and Eg is the optical band gap, α the absorption coefficient (defined by Beer–Lambert's law as α = ([2.303 × A]/d), where d and A are the sample thickness and sample absorbance, respectively.) and n is an index with different values of 1/2, 2, 3/2, and 3 for allowed direct, allowed indirect, forbidden direct and forbidden indirect electronic transitions [22]. For the estimation of the energy band gap, Tauc plots should be drawn in which $(\alpha h\upsilon)^2$ should be plotted versus hυ (photon energy) [23]. **Fig. 5** shows a plot of $(\alpha h\upsilon)^2$ vs. $h\upsilon$ illustrates the optical band gap of WO_3 and Au/WO_3 nanocomposite. The estimated optical band gap was 2.52 eV for WO_3 nanosheets and 2.41 eV for Au/WO_3 nanocomposite.

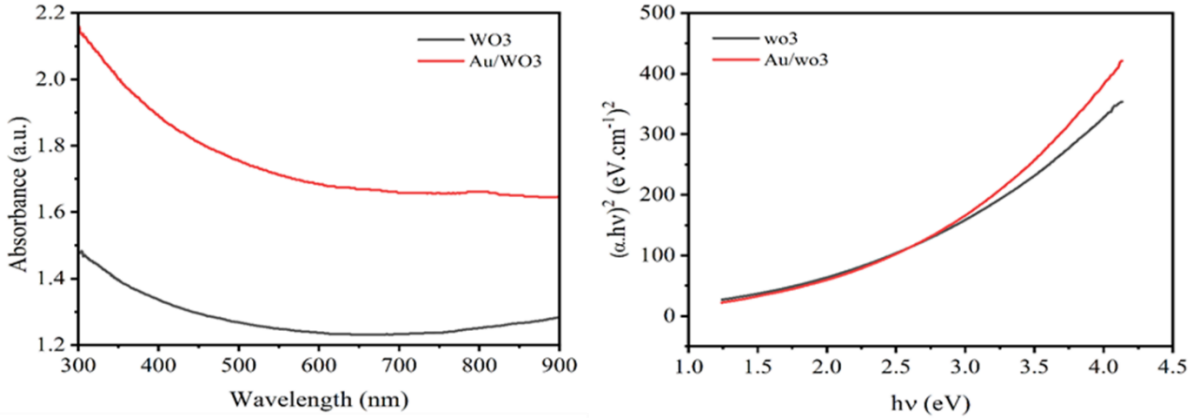

Fig. 5: The absorbance spectrum and the plot of (αhυ)2 versus photon energy of WO3 nanosheets and Au/WO3 nanocomposite

3.4. Photocatalytic activity of WO_3 nanosheets and Au/WO_3 nanocomposites

A Study of the photocatalytic activity of WO_3 nanosheets and Au/WO_3 nanocomposite was done through the degradation of MB dye under visible light irradiation. **Fig. 6** illustrations the optical absorption spectra of MB dye solution after being mixed with WO_3 nanosheets and Au/WO_3 nanocomposite in the dark and under illumination by visible light. The absorption peak of MB dye at 664 nm was found to decreases when the WO_3 nanosheets-MB dye and Au/WO_3 nanocomposites-MB dye solution was illuminated by visible light for 6min compared by the dark case. Au/WO_3 nanocomposite appeared higher degradation ratio to MB dye under illumination by visible light that could be due to the creation of metal-semiconductor hetero intersection that improves e/h carrier separation and enhances the photocatalytic activity [20, 24]. **Fig. 7** shows the photodegradation efficiency (PDE) of prepared WO_3 nanosheets and Au/WO_3 nanocomposite illuminated that for 6min. However, the Au/WO_3 nanocomposite appeared PDE of 84% while WO_3 nanosheets shows PDE of 60.1% after 6min of irradiation by visible light. Au metal exhibits local surface resonance effects that are advantageous for optical absorption, as well as a phenomenon known as plasmon-induced charge separation that has been found to be advantageous for the improvement of the photocatalytic performance of photocatalysts [24, 25]. Choi et al. [23] determined that the presence of Au in the crystal lattice of WO_3 minimizes e/h recombination and enhanced the photodegradation ratio of pollutant by approximately 50% when Au-loaded WO_3 is used.

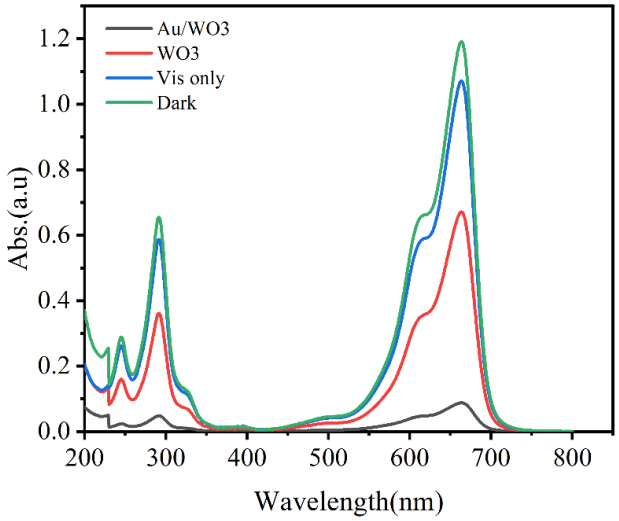

Fig. **6**: UV-Vis absorption spectra for methylene blue dye catalyzed by Au/WO_3 nanocomposite for 6min of irradiation and pH of 7.

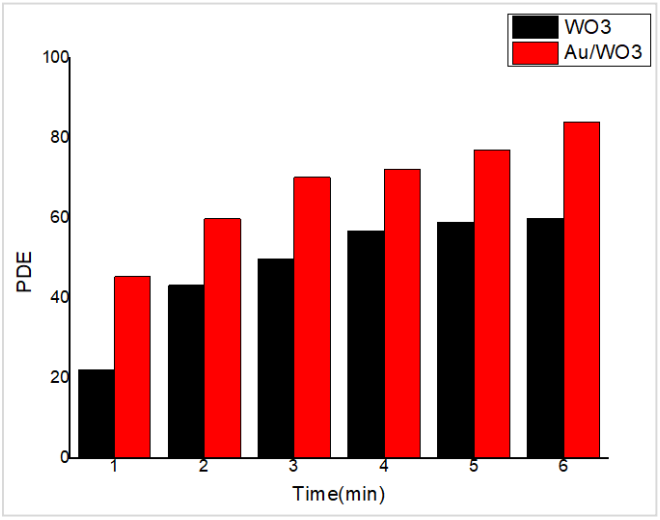

Fig. 7: Comparing between the photo degradation efficiency of MB dye catalyzed by WO_3 nanosheets and Au/WO_3 nanocomposite under visible irradiation and pH of 7.

3.5. Effect of photocatalyst weight

The influence of synthesized catalyst WO_3 nanosheets and Au/WO_3 nanocomposite quantity on the degradation of 20ppm MB dye solution was studied using a pH of 7. **Fig. 8** shows that the PDE for prepared WO_3 nanosheets and Au/WO_3 nanocomposite increases when the time of irradiation increases from 1 to 6 min. Using 0.01g of WO_3 nanosheets and Au/WO_3 nanocomposite resulted in PDE values of 12.2% and 22.2%, respectively, after 1 min of irradiation. Increasing the irradiation duration to 6 minutes, however, resulted in PDE of 56.7% for WO_3 nanosheets and 66.7% for Au/WO_3 nanocomposite, respectively. The rapid degradation of MB dye may be attributable to the structure of the catalyst, in which nanosheets have a large surface area, thereby increasing the reaction area between the dye and the catalyst. M. Awas et al. [26] found that the 25 ppm of MB dye was degraded just in one minute to 97% using 45 mg of Nb-N-TiO_2 catalyst.

However, PDE is significantly increased when dose of catalyst is increased from 0.01 to 0.1g for WO_3 nanosheets and from 0.01 to 0.05g for Au/WO_3 nanocomposite. However, increasing the photocatalyst weight of WO_3 nanosheets and Au/WO_3 nanocomposite to more than 0.1g led to a decrease in the PDE value that could be due to reduce the penetration of light inside the solution because increase turbidity of the suspension that led to decrease photoactivated of catalyst [24]. Moreover, increasing the dose of catalyst could lead to increase light scattering, screening effects, and agglomeration tendency (particle-particle interaction) that in turn leads to a decrease in light absorption by photocatalyst particles [27]. Consequently, there are fewer excited semiconductor particles. In addition, the degradation rate of the pollutant decreases at a high dosage of catalyst due to the production of fewer electron/hole pairs and hydroxyl radicals. The desired result appears to be that, even when light cannot penetrate due to a high particulate concentration, the number of active sites in the solution will increase with increasing catalyst loading. The interaction of these two paradox phenomena results in optimal catalyst concentration for photocatalytic reactions [27]. **Table 1** was listed the effect of the weight of catalysts on the PDE of MB dye solution using 20 ppm and pH of 7 dye concentration. Langmuir-Hinshelwood (L-H) model can be used to investigate the kinetic aspect of photocatalytic degradation processes as a class of heterogeneous processes. This kinetics model assumes monolayer adsorption of initial reactants or end products at the solid-liquid interface. This equilibrium adsorption mechanism is crucial to the photodegradation rate. In contrast, the equilibrium position of this adsorption process depends on the extent of oxidant or reductant adsorption. In addition, the rate-controlling phase for the entire photodegradation reaction is dependent on the adsorption of these species on the catalyst surface [22]. The kinetic rate (k) of the MB dye can be estimated by the first-order Langmuir relation formula [23,27]:

$$C = C_o e^{-kt}, \qquad 4$$

where C_o and C are the concentration of the MB dye before and after treatment, respectively, t is the time of the reaction and k is the kinetics rate of the degradation reaction. **Fig. 9** shows the - ln (C/Co) plot vs. irradiation time, the linear lines show that the photodegradation of MB dye by WO_3 nanosheets and Au/WO_3 nanocomposite samples followed the k first-order kinetic reaction. **Fig. 10** shows the kinetics of photodegradation of MB using different weight of WO_3 nanosheets and Au/WO_3 nanocomposite catalysts. The dissociation speed of the MB dye was increased with increasing the weight from 0.01 to 0.1g for WO_3 nanosheets and from 0.01 to 0.05g for Au/WO_3 nanocomposite. However, when the catalyst dose was increased from 0.01 to 0.1g, the kinetic rate value for the MB dye with a pH of 7 using WO_3 nanosheets increased from 0.1688 min^{-1} to 0.1944 min^{-1}, and then decreased when the catalyst dose was increased to 0.25g. Nevertheless, the k value increased from 0.2066 min^{-1} to 0.2133 min^{-1} as the Au/WO_3 catalyst dose was increased from 0.01 to 0.05g (**Table 2**).

3.6. Effect of pH

The pH level is a critical factor that significantly influences the efficiency of photocatalysis by regulating the adsorption of organic molecules onto the photocatalyst's surface [1]. **Fig. 11** illustrates the PDE of MB dye solution with irradiation time using different values of pH ranging from 4 to 12. The PDE value raises with a raise in the pH value and the highest degradation rate was obtained at a pH of 12 by of WO_3 nanosheets and Au/WO_3 nanocomposite. The PDE of MB dye that was catalyzed by Au/WO_3 nanocomposite was 96.2% compared by 86.4% obtained by WO_3 nanosheets after 6min of irradiation and pH of 12. The surface of the catalyst was negatively charged when pH> pHzpc (point of zero charges) while positively charged when pH< pHzpc and neutrally case when pH ≈ pHzpc [28]. In addition, a higher pH value may lead to a higher concentration of hydroxyl ions, which react with holes to form hydroxyl radicals, resulting in a rapid photocatalytic degradation rate for dyes. Due to an increase in hydroxyl ions, which promote the formation

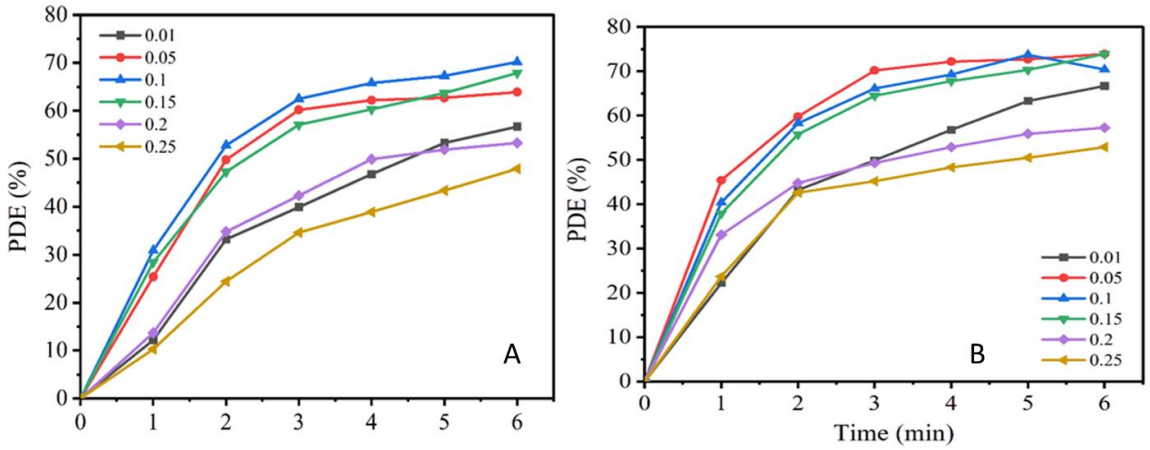

Fig. 8: Effect of (A) WO_3 nanosheets and (B) Au/WO_3 nanocomposite dose on photodegradation efficient of 20 ppm MB dye at different times

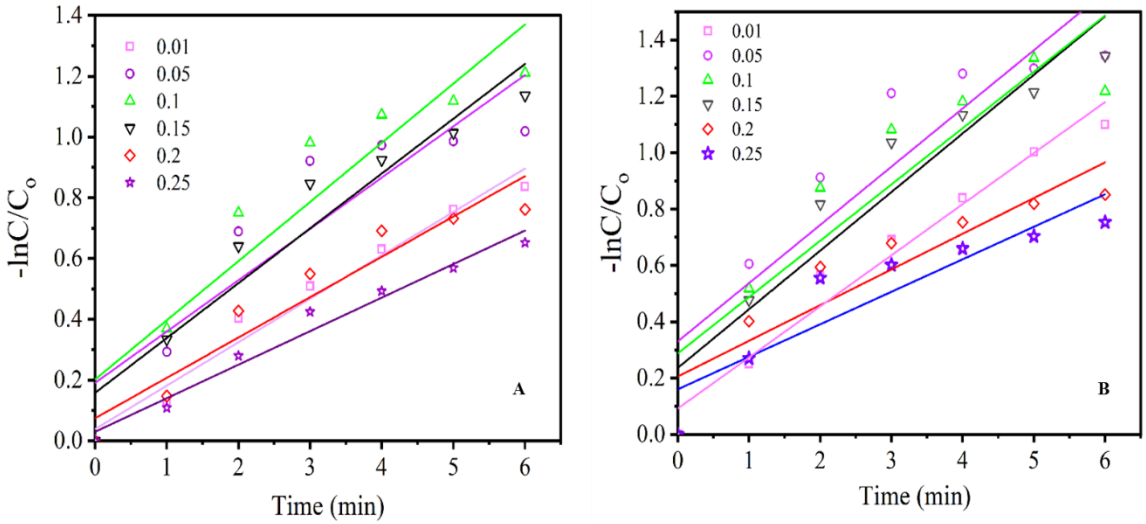

Fig. 9: Arrhenius plot for photocatalytic degradation of MB at different weight of (A) WO_3 nanosheets and (B) Au/ WO_3 nanocomposite catalysts.

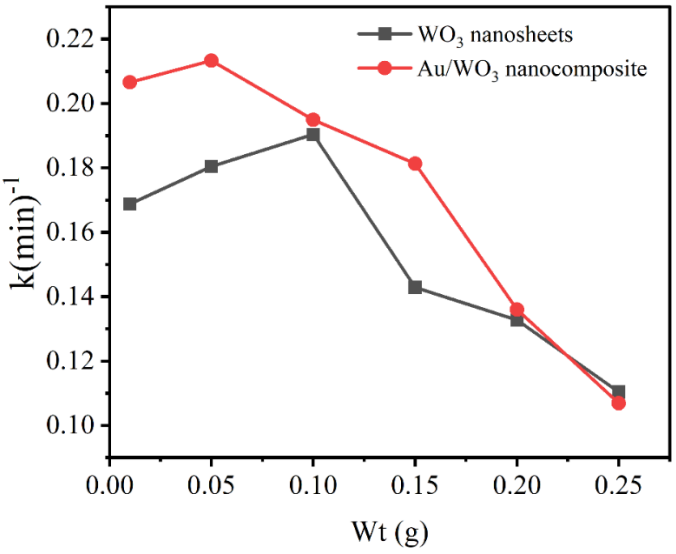

Fig. 10: Effect of weight of WO_3 nanosheets and Au/WO_3 nanocomposite catalysts on rate constant of photodegradation of MB dye solution.

Table 1: Effect the dose of WO_3 nanosheets and Au/WO_3 nanocomposite catalysts on the PDE of MB dye solution with pH of 7.

		1 min		2 min		3 min		4 min		5 min		6 min	
	Dose g	WO_3	Au/ WO_3	WO_3	Au/ WO_3	WO_3	Au/ WO_3	WO_3	Au/ WO_3	WO_3	Au/ WO_3	WO_3	Au/ WO_3
PDE %	0.01	12.2	22.2	33.2	43.2	39.9	49.9	46.8	56.8	53.3	63.3	56.7	66.7
	0.05	25.4	45.4	49.8	59.8	60.2	70.2	62.2	72.2	62.7	72.7	63.9	75.9
	0.10	30.9	40.4	52.8	58.3	62.5	66.1	65.8	69.3	67.3	73.7	70.2	73.9
	0.15	28.4	37.9	47.3	55.8	57.1	64.5	60.3	67.8	63.7	70.3	67.9	70.4
	0.20	13.7	33.1	34.8	44.8	42.3	49.3	49.9	52.9	51.9	55.9	53.3	57.3
	0.25	10.3	23.7	24.4	42.6	34.6	45.2	38.9	48.3	43.4	50.5	47.9	52.9

Table 2: The kinetic rate of MB solution using different doses of WO_3 nanosheets and Au/WO_3 nanocomposite catalysts

Catalyst dose (g)	k(min^{-1}) using WO_3 nanosheets	k(min^{-1}) using Au/WO_3 nanocomposite
0.01	0.1688	0.2066
0.05	0.1804	0.2133
0.10	0.1904	0.1947
0.15	0.1429	0.1813
0.20	0.1327	0.1360
0.25	0.1104	0.1069

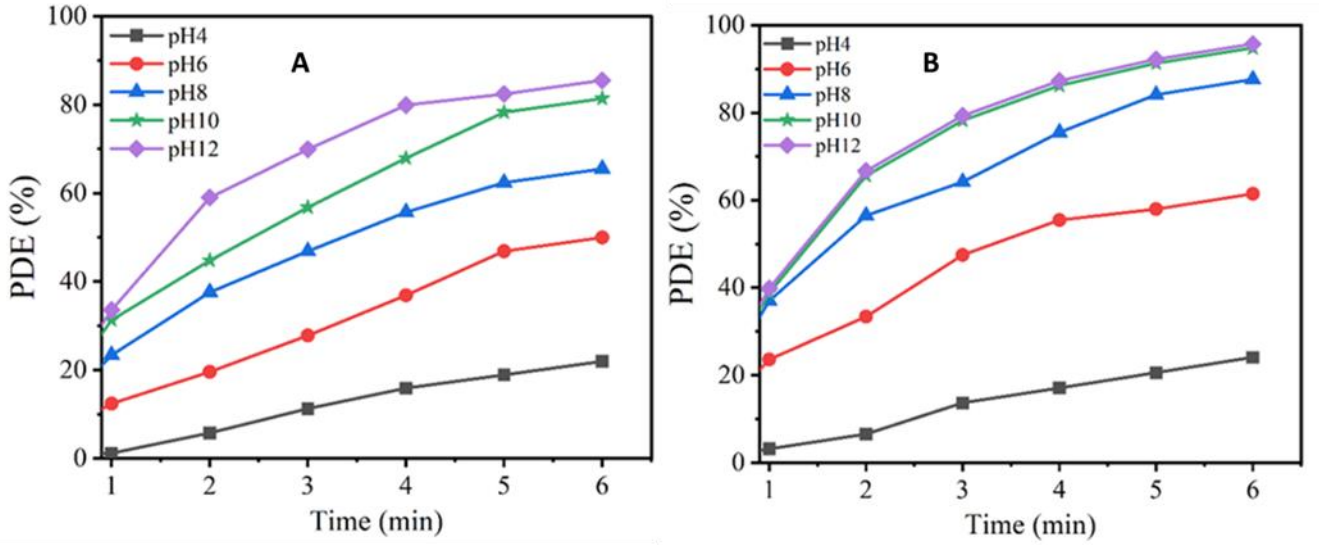

Fig. 11: Effect of pH on photodegradation efficient of 20 ppm MB dye, at 0.1g of catalysts and different times

of hydroxyl radicals, photodegradation increases in a basic environment. However, in acidic conditions, the anion can react with hydroxyl radicals to form inorganic radical ions. These inorganic radical anions are much less reactive than •OH, so they do not contribute to the decolorization of the dye [29]. On the other hand, the pKa of MB is 0.04 [20]; consequently, MB is fully ionized at a pH greater than 0.04 and exists in a cationic form[22]. However, since MB and have cationic configuration, their adsorptions are favored in the pH values higher than the pHpzc [28]. At a pH greater than pH_{ZPC}, the surface charge of the adsorbent transforms and becomes negative, resulting in a greater electrostatic attraction of the cationic dyes and an increase in the adsorption of OH–Methylene blue ions[8, 27, 29]. When the pH rises, the MB cation can replace the ion on the surface of the catalyst, resulting in an increase in adsorption via the ion exchange mechanism. The presence of an excess of H^+ ions destabilizes the basic dye and competes with cationic dye ions for the adsorption sites, which contributes to the low adsorption of MB under acidic conditions [8, 30-33]. The rate constant degradation of the MB dye solution at different pH for WO_3 nanosheets and Au/WO_3 nanocomposite

can be estimated from ln (C/C_o) plot vs. irradiation time which is shown in **Fig. 12**. **Fig. 13** shows the kinetic rate of MB catalyzed by WO_3 nanosheets and Au/WO_3 nanocomposite at different pH value. In general, the K value increased when pH value was increased and Au/WO_3 nanocomposite appeared K values higher than that obtained by WO_3 nanosheets.

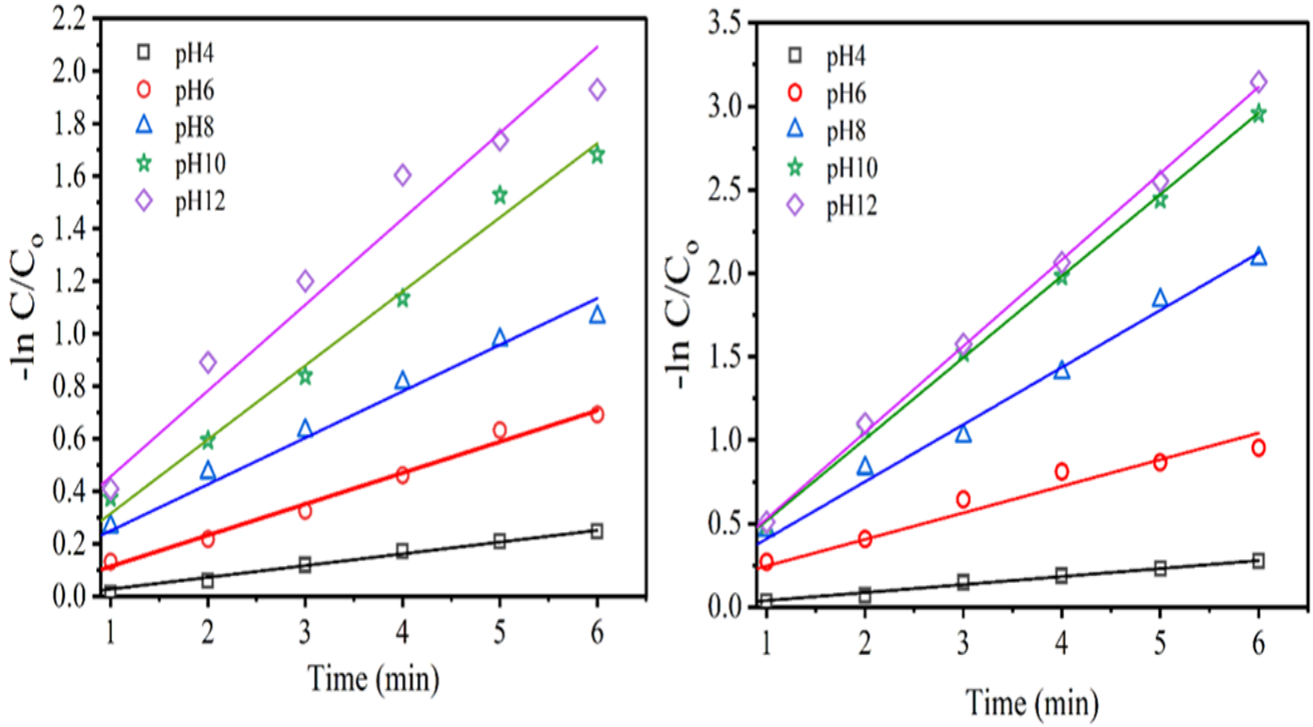

Fig. 12: Relation between ln C/C_o and time for degradation of MB on WO_3 nanosheets and Au/ WO_3 composite catalysts at different pH value.

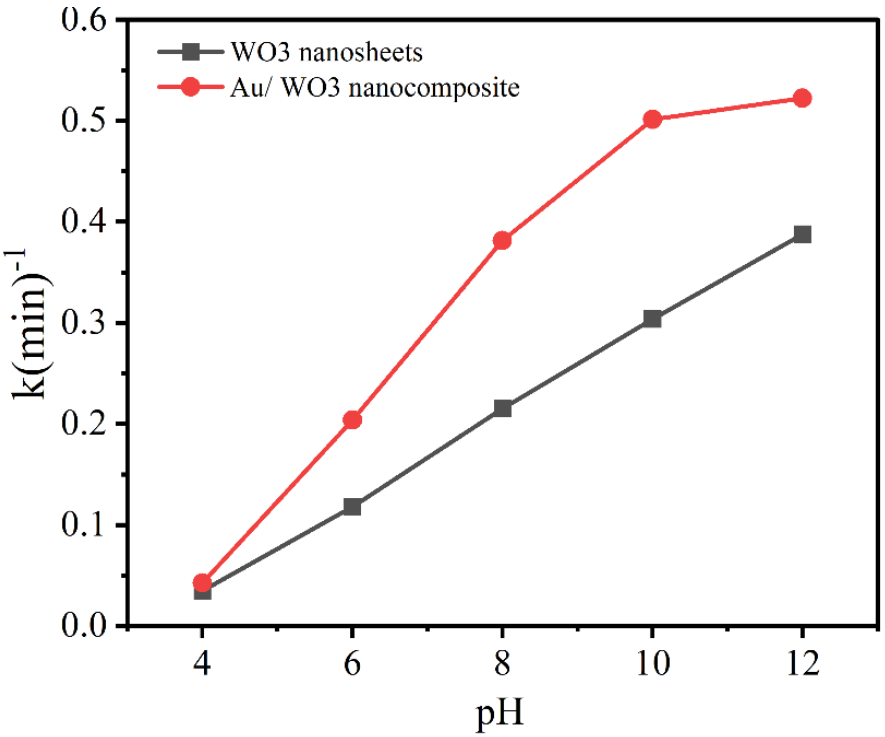

Fig. 13: The kinetic rate of MB catalyzed by WO_3 nanosheets and Au/WO_3 nanocomposite at different pH values.

4. Conclusions

The WO_3 nanosheets were prepared via the sol-gel method while Au/WO_3 composites was prepared by laser ablation technique. The prepared WO_3 nanosheets showed good crystallinity as estimated from XRD measurement. Both WO_3 nanosheets and Au/WO_3 nanocomposite exhibited a rapid rate of MB dye photodegradation under visible light. The rapid photodegradation of WO_3 nanosheets and Au/WO_3 nanocomposites that were created can potentially be attributed to the unique structure of the nanosheets. This structure increases the surface area available for the catalyst and the MB dye to interact, hence increasing the reaction rate. An Increase of the quantity of WO_3 nanosheets to 0.1g led to an elevated photodegradation rate of 70.2%, which exhibited a decreasing trend as the dose was further increased. Conversely, the photodegradation rate of the Au/WO3 nanocomposite, with a dose of 0.05g and an irradiation time of 6 minutes, demonstrated a higher photodegradation rate of 75.9%, which also decreased with an increase in dose. Increasing pH value led to increase photodegradation rate for both prepared WO_3 nanosheets and Au/WO_3 nanocomposite. The Au/WO_3 nanocomposite with a pH of 12 and an irradiation time of 6 min exhibited the maximum photodegradation rate at 95.9%. However, a higher pH value may result in a higher concentration of hydroxyl ions, which react with holes to generate hydroxyl radicals, thereby accelerating the photocatalytic degradation rate of dyes.

Acknowledgements

The authors are grateful to the Staff of the Nanotechnology Laboratory, Department of Physics, College of Science, and University of Basrah for their assistance in measuring FE-SEM images, XRD, and optical absorption.

References

[1] M.J. Kadhim, M. A. Mahdi, A. M. Selman, S.K.J. Al-Ani, J.J. Hassan, Iran. J. Catal. 13(2023) 1–21.

[2] A. Rostami‑Vartooni, L. Rostami, M. Bagherzadeh, Mater. Sci. 30(2019) 21377–21387.

[3] R. Sridharan, V. G. Krishnaswamy, K. M. Archana, R. Rajagopal, D. Thirumal Kumar, C. George Priya Doss, S. N Applied Sciences. 3(2021) 1–9.

[4] D. S. Priti Bansal, Damanjit Singh, Sep. Purif. Technol. 72(2010) 357–365.

[5] A.E. Ramírez M. Montero-Muñoz , L.L. López , J.E. Ramos-Ibarra, J. A. H. Coaquira, B. Heinrichs, C. A. Páez, Sci. Rep., 45(2021)1–9.

[6] Z. Zhang A. Zada, N. Cui, N. Liu, M. Liu, Y. Yang, D. Jiang, J. Jiang, S. Liu, Catalysts. 11(2021) 1–12.

[7] H. Derikvandi and A. Nezamzadeh-Ejhieh, J. Hazard. Mater. 9 (2016) 1–51.

[8] N. Pourshirband, A. Nezamzadeh-Ejhieh, S. Nezamoddin, S. N. Mirsattari, J. Pre-proo, 20(2020)1–51.

[9] A. Yousefi and A. Nezamzadeh-Ejhieh, Iran. J. Catal. 11(2021) 247–259.

[10] M.J. Kadhim, M.A. Mahdi, J.J. Hassan, Nanotechnology. 32(2021) 1–15.

[11] S. Yuju, T. Xiujuan, S. Dongsheng, Z. Zhiruo, and W. Meizhen, Ecotoxicol. Environ. Saf. 259(2023) 114988.

[12] Y. Xu and T. Chen, Int. J. Electrochem. Sci. 18(2023)100055

[13] A. Yousefi and A. Nezamzadeh-ejhieh, Mater. Res. Bull. 148(2022)111669.

[14] T. Ohashi, T. Sugimoto, K. Sako, S. Hayakawa, K. Katagiri, K. Inumaru, Catal. Sci. Technol. 10(2014) 1–16.

[15] M.V.C Margaux Desseigne, Véronique, M.A. Madigou, Photochem. Photobiol. 437(2023)1–17.

[16] M. Matalkeh G.K. Nasrallah, F. M. Shurrab, E.S. Al-Absi, W. Mohammed, A. Elzatahry, K. M. Saoud, Results Eng. 13(2022)100313.

[17] S. D. Khairnar, Iran. J. Catal. 8(2018)143–150.

[18] X. Song, W. Guo, Y. Guo, N. Mushtaq, M.A.K. Yousaf Shah, M.S. Irshad, P.D. Lund, M.I. Asghar , Crystals . 11(2021) 1–12.

[19] B. Manikandan, K. R. Murali, and R. John, Iran. J. Catal. 11(2021) 1–11.

[20] N. Omrani and A. Nezamzadeh-Ejhieh, Sep. Purif. Technol. 10(2019)1–87.

[21] N. Pourshirband, A. Nezamzadeh-Ejhieh, S. N. Mirsattari, J. Chem. Phys. Lett. 20 (2020)1–51.

[22] N. Pourshirband, A. Nezamzadeh-Ejhieh, J. Chem. Phys. Lett. 761(2020)1–51.

[23] H. Wook, E. Jung, S. Hong, Chem. Eng. J. 161(20210) 285–288.

[24] A. N. Rao, B. Sivasankar, V. Sadasivam, J. Mol. Catal. A. 306(2009) 77–81.

[25] M. G. Peleyeju and E. L. Viljoen, J. Water Process Eng. 40(2021) 01930.

[26] G. U. S. Awais, Muhammad, Sanya Khursheed, Rida Tehreem, Sirajuddin, Young Sun Mok, Appl. Catal. A Gen. 118764(2022)1–6.

[27] A. Nezamzadeh Ejhieh, M. Khorsandi, J. Hazard. Mater. 176(2010) 629–637.

[28] A. Nezamzadeh-Ejhieh, M. Karimi-Shamsabadi, Chem Eng. J. 228 (2013) 631–641.

[29] T. K. N Tran, V.T. Le, T. H. Nguyen, V.D. Doan, Y. Vasseghian, and H. S. Le, Korean J Chem Eng. 40(2023)1650–1660.

[30] A. Nezamzadeh and M. Khorsandi, J. Hazard. Mater. 176(2010) 629–637.

[31] A. Sobhani-Nasab, M. Eghbali-Arani, S.M. Hosseinpour-Mashkani, F. Ahmadi, M. Rahimi-Nasrabadi, V. Ameri, Iran J Catal. 10(2020) 91-99.

[32] B. Divband, A. Jodaie, and M. Khatmian, Iran. J. Catal. 9(2019) 63–70.

[33] A. Sobhani-Sasab, M. Eghbali-Arani, S. M. Hosseinpour-Mashkani, F. Ahmadi, M. Rahimi-Nasrabadi, V. Ameri, Iran. J. Catal. 10(2020) 91–99.